Chemical Engineering Science 297 (2024) 120287

Contents lists available at ScienceDirect

Chemical Engineering Science

journal homepage: www.elsevier.com/locate/ces

Online monitoring of continuous aqueous two-phase flotation (ATPF) for the development of an autonomous control strategy

Kim Carina Lohfink [a,*], Katrin Baumgärtner [b], Michel Kirsch [a], Frank Rhein [a], Moritz Diehl [c], Hermann Nirschl [a]

[a] Institute of Mechanical Process Engineering and Mechanics, Karlsruhe Institute of Technology (KIT), Strasse am Forum 8, Karlsruhe, 76131, Germany
[b] Department of Microsystems Engineering (IMTEK), University of Freiburg, Georges-Koehler-Allee 102, Freiburg im Breisgau, 79110, Germany
[c] Department of Microsystems Engineering (IMTEK) and Department of Mathematics, University of Freiburg, Georges-Koehler-Allee 102, Freiburg im Breisgau, 79110, Germany

ARTICLE INFO

Keywords:
Aqueous two-phase flotation (ATPF)
Enzyme purification
Online measurement technology
Process control

ABSTRACT

Aqueous two-phase flotation (ATPF) is a separation technique for isolating biological products such as enzymes from crude complex biosuspensions. The continuous operation mode of ATPF allows high throughput while maintaining a high separation efficiency. In this work, a laboratory plant for continuous ATPF with integrated online measurement technology is presented and ATPF experiments with the model enzyme phospholipase A_2 are performed. Three electrical conductivity probes allow real time and spatially resolved characterization of phase mixing in the flotation tank caused by rising bubbles. UV/Vis spectroscopy is used to measure the enzyme concentration online at the top phase outlet. The equilibrium concentrations in the top and bottom phase are linearly dependent on the feed concentration, revealing a constant partition coefficient. The experimental results of this work provide the basis for the development of an autonomous feedback controller for the continuous ATPF process.

1. Introduction

In recent decades, the use of biological products in industry has increased significantly. In many industrial applications, such as pharmaceuticals, food and cosmetics, high product purity is required. Downstream processing is therefore an important step in the separation and purification of biomolecules. As these biomolecules are typically sensitive species such as peptides or proteins, mild reaction conditions are required (Lee et al., 2016; Sankaran et al., 2019). Downstream processing of biomolecules requires multiple unit operations. After removal of insoluble contaminants, the product must be isolated, purified and polished. Due to the large number of steps, downstream processing of bioproducts is associated with high energy and chemical consumption (Lee et al., 2016). To combine multiple unit operations into a single process step, Bi et al. (2009) first introduced aqueous two-phase flotation (ATPF) to recover concentrated penicillin G from a fermentation broth in 2009. ATPF combines an aqueous two-phase system (ATPS) with solvent sublation (SS) (Torres-Acosta et al., 2019; Jiang et al., 2020; Li and Dong, 2010). An ATPS consists of two immiscible liquid phases that separate into a heavier bottom phase and a lighter top phase due to their different densities (Lee et al., 2016). As water is the main component of both phases, the process is highly biocompatible and the mild conditions make it particularly suitable for biological products (Lee et al., 2016; Hatti-Kaul, 2001; Ribeiro et al., 2002). ATPF is often based on a polymer-salt ATPS (Iqbal et al., 2016; Lee et al., 2016; Ribeiro et al., 2002). When both the salt and the polymer are present above critical concentrations, phase separation occurs. In general, the top phase will have a high concentration of polymer and a low concentration of salt and, in contrast, the bottom phase will have a high concentration of salt and a low concentration of polymer (Rito-Palomares and Benavides, 2017; Lee et al., 2016). This composition of the phases also results in a difference in their hydrophobicity. Commonly used polymers for the preparation of ATPS are dextran and polyethylene glycol (PEG), while phosphates, sulfates or citrates are used as salts. Although phosphates and sulfates lead to better phase separation when using PEG as a polymer due to their multivalent anions, these salts are environmentally harmful and toxic (Rito-Palomares and Benavides, 2017). To perform an

* Corresponding author.
E-mail address: kim.lohfink@kit.edu (K.C. Lohfink).

https://doi.org/10.1016/j.ces.2024.120287
Received 17 April 2024; Received in revised form 21 May 2024; Accepted 22 May 2024
Available online 27 May 2024

ATPF process, the biosuspension is mixed with the phase forming components of the bottom phase. The polymer-rich top phase is then layered on top. Gas bubbles are introduced through porous media at the bottom of the flotation tank. Hydrophobic areas of the biomolecules to be separated accumulate on the surface of the bubbles and rise with the bubbles into the top phase. For effective separation of biomolecules, the composition of the ATPS must be chosen so that the product has an increased affinity for the top phase (Rito-Palomares and Benavides, 2017; Torres-Acosta et al., 2019; Chong et al., 2020). The affinity of the molecule to the top phase is described by the partition coefficient, which is defined as the ratio of the equilibrium concentration of the molecule in the top phase to its equilibrium concentration in the bottom phase (Rito-Palomares and Benavides, 2017; Torres-Acosta et al., 2019; Chong et al., 2020; Iqbal et al., 2016). Due to the transport of the molecules into the top phase forced by the introduced bubbles, the ratio of the equilibrium concentrations is shifted towards the top phase compared to an ATPS without gassing. The resulting increased partition coefficient allows the use of a smaller top phase volume (Torres-Acosta et al., 2019). A smaller top phase volume ensures improved environmental compatibility and lower costs, as the amount of chemicals required to produce the top phase is reduced (Lee et al., 2016; Torres-Acosta et al., 2019). At the same time, a reduced volume ratio of top phase to bottom phase also increases the enrichment factor of the product in the bottom phase (Show et al., 2011, 2013; Lee et al., 2016; Chong et al., 2020; Lin et al., 2015). ATPF has already been applied to many different biomolecules. It is suitable for the separation of industrial enzymes (Show et al., 2011, 2013; Sankaran et al., 2018; Jakob et al., 2021b; Lin et al., 2015; Pakhale et al., 2013) and various therapeutically active molecules such as antibiotics (Bi et al., 2011, 2009; Jiang et al., 2020; Li and Dong, 2010), flavonoids (Bi et al., 2013, 2010; Chang et al., 2017; Chong et al., 2020), polyphenols (de Araújo Padilha et al., 2018), peptides (Jiang et al., 2019a; Md Sidek et al., 2016) and proteins (Jiang et al., 2019b, 2020, 2021).

In 2021, Jakob et al. (2021a) for the first time introduced the continuous operation of ATPF on a laboratory scale. This allows a significantly higher space-time yield compared to batch ATPF. In addition, an optimized design of a flotation cell for continuous ATPF was presented using a 3D printed prototype, taking into account the geometry of the cell as well as kinetic parameters such as the phase exchange rate and the flotation rate constant (Jakob et al., 2023). For the application, an autonomous operation of the process is desirable. An autonomous feedback control system reacts in real time to unforeseen events and disturbances during operation (Wallén, 2000; Gamer et al., 2020; Antsaklis et al., 1991). This increases product quality and yield while reducing costs and energy consumption (Gamer et al., 2020; Wallén, 2000). For the development of a predictive feedback controller, it is essential to (a) monitor the process in real time and (b) to be able to predict its future behavior. The former requires the development of appropriate online measurement technology, which is the main focus of this work. The latter requires the identification of a system model capable of reliably predicting the system behavior (Gamer et al., 2020).

To prepare the ATPF for autonomous operation, this work proposes a novel laboratory plant setup with integrated online measurement technology. In order to identify a detailed system model, spatially resolved measurements are essential to obtain local information about the process. Unlike Jakob et al. (2023), who determined phase mixing with a conductivity probe near the outlet, this work uses three electrical conductivity probes at fixed locations throughout the flotation tank. This allows, for the first time, a spatially resolved quantification of the interactions between different gassing units. In addition, the separation efficiency during continuous ATPF is determined online for the first time using UV/Vis spectroscopy. ATPF experiments with the model enzyme phospholipase A_2 show that this measurement technique works reliably and that the online measured values correspond to offline measured reference samples.

2. Material and methods

The materials and laboratory equipment used for the experimental investigations and the evaluation methods are described in the following sections.

2.1. Aqueous two-phase system (ATPS)

In this study, a polymer-salt system was used as the ATPS. Polyethylene glycol (PEG) 1000 (Ph. Eur., Carl Roth GmbH + Co. KG, Karlsruhe, Germany) was used as the polymer and trisodium citrate dihydrate (Ph. Eur., Carl Roth GmbH + Co. KG, Karlsruhe, Germany) as the salt to prepare the phases. The concentrations of the phase forming chemicals were taken from the previous work of Jakob et al. (2021a,b, 2023). The polymer-rich top phase consisted of 39.4% (w/w) PEG 1000 and 3.0% (w/w) citrate, while the bottom phase contained 0.7% (w/w) PEG 1000 and 25.8% (w/w) citrate. At the beginning of each ATPF experiment, the model enzyme pospholipase A_2 (PLP 21159, Sternenzym GmbH + Co. KG, Ahrensburg, Germany) was added to the bottom phase in concentrations of up to 1.50% (w/w). The main component of both phases was demineralized water.

2.2. Laboratory plant for continuous ATPF

Fig. 1 shows a scheme of the continuous ATPF plant used in this work with the flotation tank (see Chapter 2.2.1) in the center. On the left are the inlets for the top (TOP) and bottom phase (BOT). The bottom phase is enriched with the model enzyme phospholipase A_2, while the top phase is unloaded. Peristaltic pumps (Ismatec Reglo ICC, Cole-Parmer, St. Neots, UK) were used to ensure a uniform volume flow of both phases. The volume flow of the top phase was 1.67 ml/min and that of the bottom phase was 8.33 ml/min for all experiments, resulting in a residence time of 60 min of each phase in the flotation tank. Three gassing units at the bottom introduced air into the flotation tank. Each consists of a 3D-printed holder into which a circular twill weave (TopMesh TM10, Spoerl, Sigmaringendorf, Germany) with a nominal pore size of 10 µm and a diameter of 2 cm was bonded using a two-component adhesive (UHU plus endfest, UHU GmbH + Co. KG, Buehl, Germany). The gas flow rates were individually controlled by mass flow controllers (SLA55800, Brooks Instrument, Dresden, Germany). In all ATPF experiments, 500 ml of enzyme-enriched bottom phase was added to the flotation tank and 100 ml of unloaded top phase was carefully layered on top. This results in a volume ratio of top to bottom phase of 0.2.

The top and bottom phase outlets were designed to eliminate the need for additional peristaltic pumps at either outlet. The top phase was discharged via an overflow edge and then passed through a horizontally mounted hose, while the bottom phase left the flotation tank via a siphon design. This was done by using a hose to create a siphon shape and adjusting its maximum height accordingly. To determine the enzyme concentration in real time during ATPF experiments, a UV/Vis spectrometer was installed at the top phase outlet. Three electrical conductivity probes were integrated into the system to additionally characterize the phase mixing during the process. The UV/Vis spectrometer and the evaluation of the phase mixing with the electrical conductivity probes are described in detail in the Chapter 2.2.2.

The control units, i.e. the peristaltic pumps and the three gassing units were controlled by LabVIEW (version 21.1.2, National Instruments, Austin, Texas, US). This software also reads the measurements from the electrical conductivity probes and records them at manually adjustable times.

2.2.1. Flotation tank

Jakob et al. (2023) developed a 3D printed prototype with an optimized apparatus design for continuous ATPF. Their geometry was taken into account when manufacturing the flotation tank used in this work.

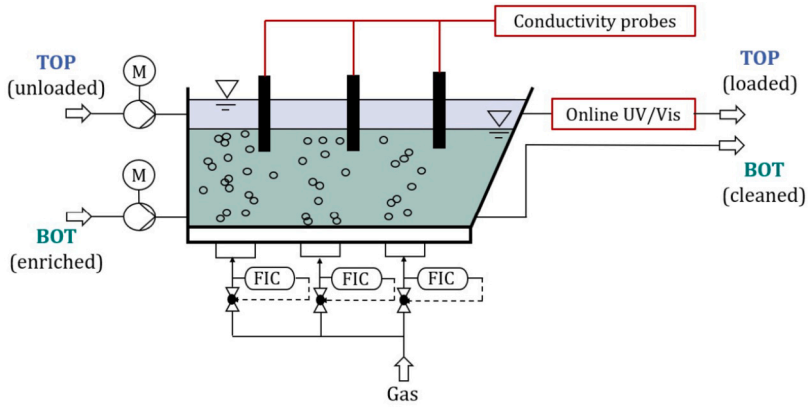

Fig. 1. Setup of the laboratory plant for continuous ATPF.

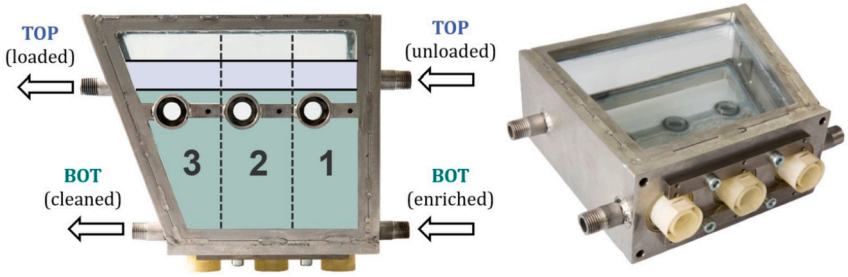

Fig. 2. Flotation tank used for continuous ATPF experiments from the rear (left) and from the bottom-left-front (right).

Fig. 2 shows the flotation tank from different perspectives. The tank consists of a welded stainless steel frame. It has openings for the inlets and outlets of the two phases, the three gassing units and electrical conductivity probes. Glass panels were glued to the front and back of the flotation tank to allow visual characterization of the process. On the outlet side, the tank is inclined 20 degrees to allow a 4.5 cm long section without gassing. This reduces the phase mixing in this area in order to prevent the bottom phase from entering the top phase outlet.

The flotation tank is conceptually divided into three separate compartments without actual physical separation between the compartments. The numbering of each compartment is shown on the left in Fig. 2, with compartment 1 on the inlet side, compartment 2 in the middle, and compartment 3 on the outlet side. Each of these compartments contains a gassing unit and an electrical conductivity probe that is mounted horizontally slightly offset from the gassing unit. This offset minimizes the influence of gas bubbles on the electrical conductivity measurements. Contrary to what is shown in Fig. 1, the conductivity probes are not inserted into the flotation tank from above, but through the openings provided in the steel frame of the flotation tank, so that they are integrated into the bottom phase at fixed positions at a 90 degree angle (see Fig. 2 left). The individual gas flow rates in each compartment are combined into gas flow rate combinations. The gas flow rates are given in ml/min, separated by dashes, where the first number is the gas flow rate in compartment 1, the second is the gas flow rate in compartment 2, and the third is the gas flow rate in compartment 3.

2.2.2. Online measurement technology for real time monitoring of process parameters

Online measurement technology was integrated into the laboratory ATPF plant to monitor various process parameters. To determine the phase mixing, three electrical conductivity probes (InPro7100i, Mettler Toledo, Columbus, Ohio, US) were installed 1 cm below the phase interface in the bottom phase (see Fig. 2 left). Analogous to Jakob et al. (2023) a calibration curve was created to determine the relationship between the electrical conductivity and the volume fraction of dispersed top phase in the bottom phase. This takes advantage of the significant difference in electrical conductivity between the two phases due to the different salt concentrations. When the flotation tank is gassed, the top phase displaces the citrate ions of the bottom phase near the electrical conductivity probes, resulting in a reduced measured electrical conductivity. To determine the calibration curve, different volume fractions of the top in bottom phase were placed in a beaker and completely mixed with a magnetic stirrer while the electrical conductivity was measured with the electrical conductivity probes. Volume fractions ranging from 0% to 22% top to bottom phase were used to establish a reliable calibration curve.

A UV/Vis spectrometer (HR-4UVV250-25, Ocean Optics B.C., Ostfildern, Germany) was installed at the top phase outlet for real time determination of the enzyme concentration. The loaded top phase leaving the flotation tank passes through a bubble separator and then through a flow cell. The flow cell is in turn is connected to the light source by a fiber optic cable and to the spectrometer on the opposite side by a second fiber optic cable. Light in the UV/Vis wavelength range hits the sample and the spectrometer measures the absorbance caused by the sample. The corresponding enzyme concentration is determined from calibration between the enzyme concentration and absorbance.

2.3. Evaluation methods of measured process parameters

The bubble surface flux S_b is used to determine the bubble surface input per unit time related to the gassed sectional area A_C. S_b is calculated according to

$$S_b = \frac{6 \cdot \dot{V}_g}{A_C \cdot d_{3,2}}. \tag{1}$$

Here, $\dot{V}_g$ is the gas flow rate and $d_{3,2}$ is the Sauter mean diameter of the gas bubbles (Xu et al., 1991). The values for $d_{3,2}$ at different gas flow rates were taken from Jakob et al. (2021b). To calculate the S_b value for a flotation tank with multiple gassing units, the S_b was determined separately for each gassing unit and then the values were added together.

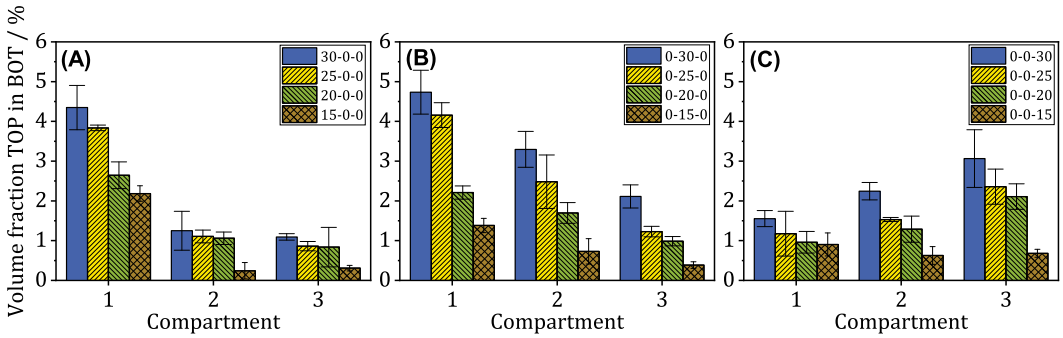

Fig. 3. Separate gassing of individual compartments to investigate the influence on the other two compartments. **(A)** Gassing only in compartment 1. **(B)** Gassing only in compartment 2. **(C)** Gassing only in compartment 3.

The enzyme concentration at the outlet of the top phase was measured online using the UV/Vis spectrometer. The corresponding enzyme concentration at the bottom phase outlet was calculated from the measured top phase concentration using a mass balance. The mass balance states that the enzyme mass m_{enz} present in the entire flotation tank is equal to the sum of the enzyme mass $m_{enz,TOP}$ present in the top phase and the enzyme mass $m_{enz,BOT}$ present in the bottom phase:

$$m_{enz} = m_{enz,TOP} + m_{enz,TOP} \tag{2}$$

If the expressions for the enzyme mass of both phases are replaced by the product of the volume of the respective phase $V_{TOP/BOT}$ in the flotation tank, its density $\rho_{TOP/BOT}$ and the enzyme concentration present at time t $x_{TOP/BOT,t}$, then after transformation for the enzyme concentration in the bottom phase $x_{BOT,t}$ at time t, the following is obtained:

$$x_{BOT,t} = \frac{m_{enz} - V_{TOP} \cdot \rho_{TOP} \cdot x_{TOP,t}}{V_{BOT} \cdot \rho_{BOT}} \tag{3}$$

This equation can be used to calculate the concentration in the bottom phase from the measured enzyme concentration in the top phase, assuming that there is no accumulation of enzyme in the flotation tank.

For characterizing the performance of a flotation experiment, the separation efficiency E was determined. It describes the amount of enzyme transported from the bottom phase to the top phase at time t and is calculated by

$$E = \left(\frac{x_{TOP,t}}{x_{TOP,max}} \right) \cdot 100\%, \tag{4}$$

with the enzyme concentration $x_{TOP,t}$ in the top phase at time t and the maximum concentration $x_{TOP,max}$ that occurs in the top phase when the enzyme is completely transferred from the bottom to the top phase.

The kinetics of ATPF are described by the following dynamics using first order kinetics (Li and Dong, 2010; Bi et al., 2011):

$$\frac{dx_{BOT}}{dt} = -k \cdot x_{BOT} \tag{5}$$

Here, x_{BOT} is the enzyme concentration in the bottom phase and k is the flotation rate constant. Combining Equation (5) with (4) results in Jakob et al. (2021b, 2023)

$$E(t) = E_{\infty} \cdot \left(1 - e^{-kt}\right) \cdot 100\%. \tag{6}$$

This equation was used to fit the separation efficiency curve and allows the determination of the equilibrium separation efficiency E_{∞} and the flotation rate constant k for the respective ATPF experiment. Equation (6) confirms that the separation efficiency asymptotically approaches the equilibrium separation efficiency during the process (Lee et al., 2016).

3. Results and discussion

3.1. Individual gassing of each compartment and its effect on phase mixing in the flotation tank

The implementation of electrical conductivity probes at fixed locations in all three compartments allows for the first time spatially resolved monitoring of flow and mixing conditions. To characterize the influence of gassing in each compartment on the other two compartments, each compartment was gassed individually and the phase mixing in all compartments was investigated. Gas flow rates between 15 ml/min and 30 ml/min were used. At individual gas flow rates above 30 ml/min, complete mixing of the two phases was observed, leading to a fully diffusion controlled process and thus to aqueous two-phase extraction (ATPE). When both phases are completely mixed in the flotation tank, the measured volume fraction of dispersed top phase in the bottom phase is 20% due to their volume ratio of 0.2. Fig. 3 shows the volume fractions of dispersed top phase in bottom phase measured in each compartment during individual gassing of each compartment.

If gassing is performed only in compartment 1 (see Fig. 3A), the volume fraction of dispersed top phase in bottom phase is highest in this compartment. At a gas flow rate of 30 ml/min, the volume fraction of top phase in bottom phase is 4.25 ± 0.56% and at 15 ml/min the volume fraction is 2.19 ± 0.19%. The effects of individual gassing of compartment 1 can also be seen in compartment 2 and 3. At a gassing rate of 30 ml/min, the volume fraction of top phase in bottom phase is 1.25 ± 0.49% in compartment 2 and 1.09 ± 0.08% in compartment 3. Due to the small difference between the volume fractions of top phase in bottom phase in compartments 2 an 3, it can be concluded that the gassing of compartment 1 influences the phase mixing in compartment 2 and 3 almost equally. The same observation applies when using different gas flow rates in compartment 1, as shown in Fig. 3A.

If instead only compartment 2 is gassed (see Fig. 3B), the system behaves differently. In this case, the phase mixing is greatest not in the gassed compartment 2, but in the adjacent compartment 1. In compartment 2, the volume fraction of top phase in bottom phase at a gas flow rate of 30 ml/min is 3.30 ± 0.45%, while in the compartment 1 it is 4.73 ± 0.55%. The lowest value was measured in compartment 3 with 2.11 ± 0.29%. This behavior is evident for all gas flow rates used for gassing in compartment 2. From the measured values, an increased transport of top phase into compartment 1 can be determined when gassing in compartment 2. As a result, gassing in compartment 2 causes the top phase to flow back against the direction of phase exchange.

Fig. 3C shows the respective volume fractions of top phase in bottom phase during individual gassing of compartment 3 at different gas flow rates. Analogous to the gassing of compartment 1, the phase mixing is highest in the gassed compartment and lowest in the most distant compartment 1. It can also be seen that the volume fraction of top phase in bottom phase is lower at the same gas flow rate than when the other two compartments are gassed. At a gas flow rate of 30 ml/min, the de-

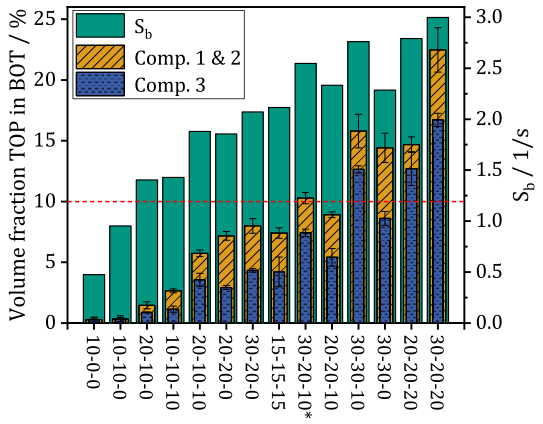

Fig. 4. Influence of gas flow rate combinations on the bubble surface area flux S_b and phase mixing.

termined volume fraction of top phase in bottom phase in compartment 3 is 3.07 ± 0.73%. Compared to the value of 4.34 ± 0.56% for the volume fraction in compartment 1 at a gassing rate of 30 ml/min, there is a difference of 1.26%. Due to the geometry of the flotation tank with the inclined side wall at the outlet, compartment 3 has a special position compared to the other two compartments. The geometry of the flotation tank means that the cross-sectional area of compartment 3 increases with increasing height. This means that the proportion of gassed area in compartment 3 is lower than in compartments 1 and 2, resulting in an overall reduction in phase mixing. The results confirm that phase mixing can be reduced by a sloped side wall on the outlet side. It is desirable to minimize phase mixing in compartment 3 in order to prevent the bottom phase from entering the outlet of the top phase.

3.2. Influence of gas flow rate combinations on phase mixing

The cell design allows separate gassing of each compartment. High phase mixing is required for optimal separation and enrichment of phospholipase A_2 in the top phase as it increases the diffusive transport of the enzymes between both phases due to a larger phase interface compared to the ATPS at rest. High phase mixing is achieved by increasing the gas flow rate in the respective compartment. According to Equation (1), an increased gas flow rate leads to an increase in the bubble surface area flux S_b. Jakob et al. (2021b) found a linear correlation between the S_b value and the flotation rate constant k. Accordingly, the flotation rate constant increases with increasing S_b, which provides for a higher flotation speed. Equation (6) shows that the equilibrium separation efficiency is reached faster at a higher flotation rate constant, which is advantageous for continuous ATPF. High phase mixing is desirable only in compartments 1 and 2. In compartment 3, excessive phase mixing prevents phase separation and bottom phase entering the top phase outlet. Preliminary ATPF experiments showed that a volume fraction of 10% dispersed top phase in bottom phase in compartment 3 means that the phase mixing is too high for optimal phase separation and should not be exceeded. With an electrical conductivity probe in each of the three compartments, it is possible to measure the phase mixing in a spatially resolved manner and thus optimize the gas input.

Fig. 4 shows the averaged volume fractions of top phase in bottom phase in the first two compartments (yellow bars), the volume fraction in the third compartment (blue bars) and the S_b value calculated from the gassing combination (green bars) at different gas flow rate combinations.

Using the gas flow rate combination 10-0-0, the average volume fraction of dispersed top phase in bottom phase in compartment 1 and 2 is only 0.28 ± 0.21%. Of all the gas flow rate combinations tested, this is the one with the lowest phase mixing in the first two compartments. With increasing total gas flow rate, the volume fractions of top phase in bottom phase increase in all three compartments. Accordingly, at a total gas flow rate of 30 ml/min and the gassing combination 10-10-10, the average volume fraction of top phase in bottom phase in the first two compartments is 5.73 ± 0.27% and at the total gas flow rate of 60 ml/min and the gassing combination 20-20-20 14.68 ± 0.63%. At the same time, the volume fraction of top phase in bottom phase in compartment 3 increases from 1.14 ± 0.26% at 10-10-10 to 12.71 ± 1.29% at 20-20-20. It can be seen that with the same gas flow rates in the first two compartments, the volume fraction of top phase in bottom phase is greater in all three compartments when the gas flow rate in the third compartment is increased. For example, with the combinations 20-20-0, 20-20-10 and 20-20-20 the volume fraction of top phase in bottom phase in the third compartment increases from 2.93 ± 0.17% for the combination 20-20-0 to 12.71 ± 1.39% for the combination 20-20-20. At the same time, the average value over the first two compartments increases from 7.17 ± 0.35% for 20-20-0 to 14.68 ± 0.63% for 20-20-20. This observation confirms the results in Fig. 3, as the influence of gassing one compartment on the other two compartments is also evident here. According to Equation (1), the S_b values for the tested gas flow rate combinations are between 0.48 1/s for 10-0-0 and 2.97 1/s for the gas flow rate combination 30-20-20.

The results show that the total gas flow rate alone is not a sufficient indicator of the flow conditions in the flotation tank. Rather, the combination of gas flow rates in all three compartments is critical. Of the gas flow rate combinations shown in Fig. 4, three do not meet the previously set condition of not exceeding a volume fraction of 10% dispersed top phase in bottom phase (see red dashed line) in the third compartment. These are the gas flow rate combinations 30-30-10, 20-20-20 and 30-20-20. Of the remaining gas flow rate combinations, 30-20-10 has the highest value for S_b with 2.55 1/s which, according to the linear increase of the flotation rate constant with S_b found by Jakob et al. (2021b), is expected to yield the fastest flotation. However, the gas flow rate combination 30-30-0 has the highest average volume fraction of top phase in bottom phase of 14.41 ± 1.21% in the first two compartments. This means that the diffusive transport is expected to be the largest in the combination 30-30-0 due to the significantly increased phase interface area. Since phase mixing in the compartment 3 is also lower for 30-20-10 than for 30-30-0, the 30-20-10 gas flow rate combination was used for the flotation experiments described below.

3.3. Real-time determination of the enzyme concentration using online UV/vis spectroscopy

The main goal of ATPF is to achieve a high enzyme concentration in the top phase, i.e. a high separation efficiency. To characterize the mass transfer from the bottom to the top phase during ATPF, it is therefore useful to determine the time-dependent enzyme concentration profiles in both phases at the outlets. In this work, the enzyme concentration at the outlet of the top phase was measured online for the first time using UV/Vis spectroscopy (see Chapter 2.2.2). The enzyme concentration in the bottom phase can be calculated from the measured values using a mass balance equation (see Equation (3)), assuming that there is no enzyme accumulation in the flotation tank, e.g. on the tank walls. Fig. 5 shows the enzyme concentrations determined online at the outlet of the top phase (Fig. 5A) and the bottom phase concentrations calculated via the mass balance equation (Fig. 5B) using feed concentrations of 1.00% (w/w), 1.25% (w/w) and 1.50% (w/w). Based on the results of Chapter 3.2, the gas flow rate combination 30-20-10 (marked with * in Fig. 4) was used in the experiments, as this has the largest S_b value with simultaneously low phase mixing in compartment 3. Parallel to the online measurement of the top phase enzyme concentration, samples were taken from the outlet of the bottom phase at different times and the enzyme concentration was determined offline via UV/Vis spectroscopy to ensure the accuracy of the online measurements and to validate the mass balance. The enzyme concentrations in the bottom phase determined in this way are shown as colored markers in Fig. 5B.

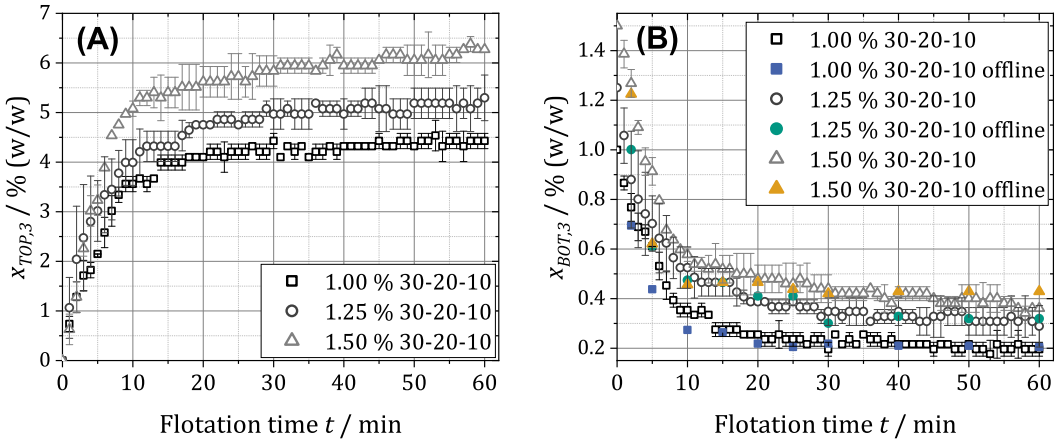

Fig. 5. Time-dependent enzyme concentration profiles in the top phase **(A)** and bottom phase **(B)** during continuous ATPF. The gas flow rate combination 30-20-10 and a residence time of 60 min was used in all experiments. The feed concentrations varied between 1.00% (w/w), 1.25% (w/w) and 1.50% (w/w).

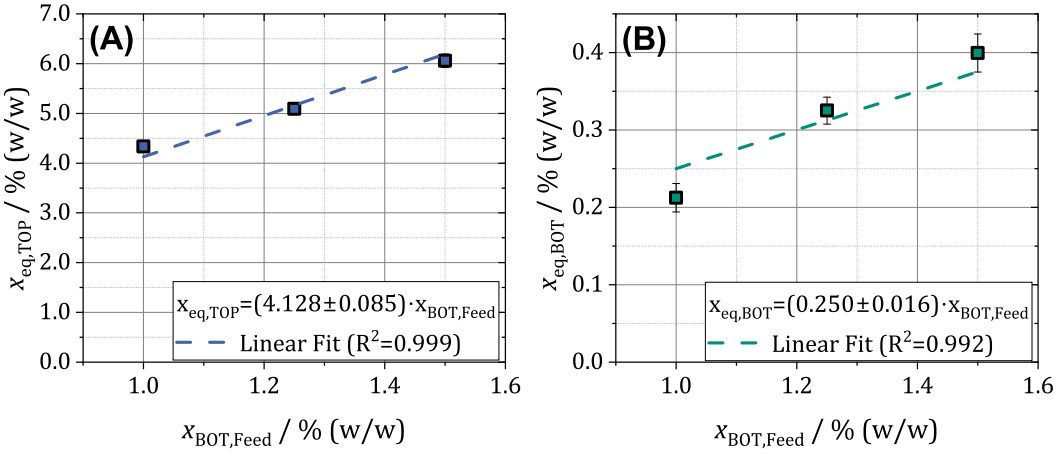

Fig. 6. Equilibrium concentrations at different feed concentrations in the top phase **(A)** and bottom phase **(B)**. A linear fit was performed in each case and the fit function was determined.

Table 1
Summary of measured parameters during continuous ATPF at different feed concentrations.

$x_{BOT,Feed}$ in % (w/w)	1.00	1.25	1.50
$x_{eq,TOP}$ in % (w/w)	4.34 ± 0.10	5.09 ± 0.10	6.06 ± 0.14
$x_{eq,BOT}$ in % (w/w)	0.21 ± 0.02	0.33 ± 0.02	0.40 ± 0.02
E_∞ in %	78.76 ± 1.84	74.00 ± 1.40	73.37 ± 1.64
k in 1/min	0.161 ± 0.003	0.165 ± 0.005	0.165 ± 0.004

Prior to starting the experiments, both phases are placed in the flotation tank. At time $t = 0$ min, the enzyme is present in the feed concentration in the bottom phase, while the top phase contains no enzyme. Once the experiment is started by starting the peristaltic pumps and the gassing units via LabVIEW, the enzyme concentrations in the bottom and top phase change over time. The mass transfer from the bottom phase to the top phase during the ATPF is caused both by the flotation itself, i.e. the transport of the molecules on the rising bubbles, and by diffusion across the phase interface. This mass transport causes the enzyme concentration in the bottom phase to decrease during flotation, while it increases in the top phase. After 30 min, an equilibrium concentration is reached in both phases. The equilibrium concentrations in top and bottom phase are defined as the mean of all values after 30 min of flotation time and are listed in Table 1.

The values show increasing equilibrium concentrations in both phases with increasing feed concentration. In Fig. 6 the equilibrium concentrations in the top phase $x_{eq,BOT}$ (Fig. 6A) and in the bottom phase $x_{eq,TOP}$ (Fig. 6B) are plotted against the feed concentration. A linear fit through the origin is performed in each case, and the corresponding equations are given in Fig. 6.

The transport mechanisms of flotation and diffusion are responsible for the increasing equilibrium concentrations with increasing feed concentration. The mass transfer of enzymes from the bottom phase to the top phase by flotation is caused by the accumulation of enzymes on the surface of the bubbles. Since there are more enzymes in the bottom phase, a higher concentration in the bottom phase increases the probability of collision between the bubbles and the enzymes. At the same time, there is a higher concentration gradient between the bottom phase and the top phase at the beginning of the flotation experiments with higher feed concentrations. This additionally increases the absolute mass transfer by diffusion across the phase interface. At equilibrium after 30 minutes, a partition coefficient of $K_p = 16.51 \pm 1.40$ is achieved, regardless of the feed concentration. This means that the loading of the bubbles with enzymes increases as the feed concentration increases. This observation can be confirmed by a mass balance equation of the top phase. The time variation of the enzyme concentration in the top phase is 0 at steady state after 30 min and

$$\frac{dx_{TOP}}{dt} = 0 = \frac{\dot{m}_{eq,enz} - \dot{m}_{out} x_{eq,TOP} - \dot{m}_{eq,diff}}{m_{TOP}}, \quad (7)$$

with the total enzyme mass flow $\dot{m}_{eq,enz}$ entering the top phase from the bottom phase by flotation and diffusion, the total mass flow $\dot{m}_{out}$ leaving the flotation tank through the top phase outlet, and the enzyme

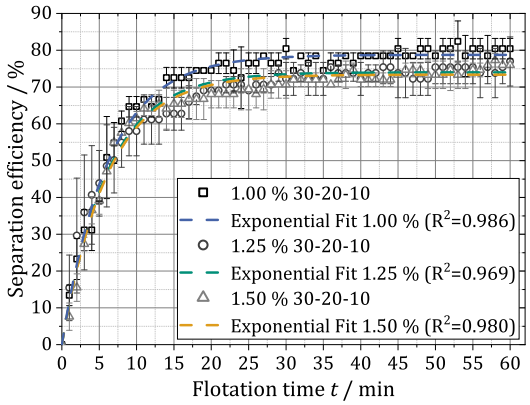

Fig. 7. The separation efficiency as a function of the flotation time using different feed concentrations.

mass flow $\dot{m}_{eq,diff}$ leaving the top phase by diffusive transport across the phase interface. $\dot{m}_{eq,diff}$ can be formulated using the diffusion coefficient D and the equilibrium concentrations in top phase and bottom phase $x_{eq,TOP}$ and $x_{eq,TOP}$ as follows:

$$\dot{m}_{eq,diff} = D(x_{eq,TOP} - x_{eq,BOT}) \tag{8}$$

By inserting Equation (8) into Equation (7), the following is obtained:

$$x_{eq,TOP} = \frac{\dot{m}_{enz}}{\dot{m}_{out} + D(1 - \frac{1}{K_p})} = \frac{\dot{V}_g b_{enz}}{\dot{m}_{out} + D(1 - \frac{1}{K_p})} \tag{9}$$

In this equation the ratio of $x_{eq,TOP}$ to $x_{eq,BOT}$ is replaced by the partition coefficient K_p. In addition, $\dot{m}_{enz}$ is described by the product of the gassing rate $\dot{V}_g$ and the volume specific enzyme loading b_{enz}. Equation (9) shows that for a constant value of K_p the bubble loading increases proportionally with $x_{eq,TOP}$ if $\dot{V}_g$ remains constant. As the same gas flow rate combination is applied in all experiments, the bubble surface area flux has a value of 2.55 1/s (see Chapter 3.2). The available bubble surface area can therefore be considered as constant in all ATPF experiments. The experimental results allow conclusions to be drawn about the bubble loading. Due to the constant equilibrium coefficient at the feed concentrations tested in this work between 1.00% (w/w) and 1.50% (w/w), complete saturation of the bubble surfaces has not yet been achieved at these feed concentrations. To further optimize the enzyme separation, it is therefore possible to run even higher concentrations as this would increase the absolute amount of enzyme that is separated per unit time. Once the feed concentration is reached at which complete saturation of the bubble surfaces is achieved for the prevailing process parameters (i.e. residence time and gas flow rate combination), a further increase in the feed concentration leads to a reduction in separation efficiency as some of the enzymes remain in the bottom phase and leave the flotation tank via the bottom phase outlet.

The separation efficiency can be calculated from the enzyme concentration in the top phase at time t using Equation (4). Fig. 7 shows the separation efficiency as a function of the flotation time. To determine the flotation rate constant k according to Equation (6), an exponential fit function is applied in each case.

In Table 1 the flotation rate constant k as well as the equilibrium separation efficiency E_∞ for each tested feed concentration are listed. It can be seen that k is almost identical for the feed concentrations 1.00% (w/w), 1.25% (w/w) and 1.50% (w/w). This means that equilibrium is reached at the same rate for these feed concentrations. The equilibrium separation efficiencies E_∞, i.e. the average of the separation efficiencies from 30 minutes of flotation time, also remain almost constant at the feed concentrations used. This observation can again be confirmed using appropriate equations. For the maximum achievable enzyme concentration $x_{TOP,max}$ in the top phase, which is reached when the enzyme is completely transferred to the top phase, the following applies due to mass conservation:

$$x_{TOP,max} = \frac{x_{eq,TOP} V_{TOP} + x_{eq,BOT} V_{BOT}}{V_{TOP}} = \frac{x_{eq,TOP}(V_{TOP} + V_{BOT}\frac{1}{K_p})}{V_{TOP}} \tag{10}$$

The equilibrium efficiency E_∞ is calculated from the equilibrium concentration in the top phase $x_{eq,TOP}$ and $x_{TOP,max}$ according to

$$E_\infty = \frac{x_{eq,TOP}}{x_{TOP,max}}. \tag{11}$$

Inserting Equation (10) into Equation (11) results in

$$E_\infty = \frac{V_{TOP}}{V_{TOP} + V_{BOT}\frac{1}{K_p}}. \tag{12}$$

The relationship between K_p and E_∞, described by Equation (12), shows that E_∞ must also be constant if K_p is constant.

4. Conclusion

Online and spatially resolved measurement technology is critical to the characterization and autonomous feedback control of continuous ATPF. Electrical conductivity measurements can be used to evaluate phase mixing effects caused by rising bubbles by exploiting the significant difference in electrical conductivity between the bottom and top phase. The gas flow rates in each compartment affect the amount of top phase dispersed in the bottom phase as well as the bubble surface area flux S_b. The novel setup presented in this work allows for the first time the quantification of the interaction between spatially resolved gassing and spatially resolved phase mixing. This allows the optimization of the gas input by adjusting the individual gassing rates of the three separately controllable gassing units. To maximize the bubble surface area flux and to increase the phase interface for diffusive transport, high phase mixing in compartments 1 and 2 is desirable. Low phase mixing in compartment 3 prevents the bottom phase from entering the top phase outlet. Of all the gas flow rate combinations tested in this work, 30-20-10 has the largest S_b value of 2.55 1/s while maintaining a volume fraction of dispersed top phase in bottom phase below 10% in compartment 3. Continuous ATPF experiments with the model enzyme phospholipase A_2 at the gas flow rate combination 30-20-10 show that the enzyme concentration in the top phase initially increases exponentially with time and reaches an equilibrium value after 30 min, regardless of the feed concentration. The equilibrium concentrations are linearly dependent on the feed concentration, revealing a constant partition coefficient. This means that the loading of the bubble surface increases with increasing feed concentration, which can be confirmed by a mass balance. Thus, the feed concentration can be further increased to obtain a more efficient ATPF process. The experimental results of this work therefore allow conclusions to be drawn about the bubble loading and provide information about its kinetics.

In summary, the laboratory system for continuous ATPF presented in this work shows that local phase mixing and the separation efficiency can be monitored in real time using suitable online measurement technology. The experimental results of this work form the basis for the identification of a process model which is necessary for the development of a suitable control strategy for continuous ATPF. To validate the model and obtain necessary kinetic parameters, further experimental investigations are required to characterize the dynamic process behavior. The development of a connectivity between online measurement data and the control units in combination with a closed-loop control system enables an autonomously controllable ATPF process where the control variables are dynamically adapted to the measured variables in order to ensure a consistently high separation efficiency.

CRediT authorship contribution statement

Kim Carina Lohfink: Writing – review & editing, Writing – original draft, Visualization, Investigation, Data curation, Conceptualization. **Katrin Baumgärtner:** Writing – review & editing, Methodology, Investigation. **Michel Kirsch:** Methodology, Investigation. **Frank Rhein:** Writing – review & editing, Supervision, Methodology. **Moritz Diehl:** Supervision, Resources, Project administration, Funding acquisition. **Hermann Nirschl:** Writing – review & editing, Supervision, Resources, Project administration, Funding acquisition.

Declaration of competing interest

The authors declare that they have no known competing financial interests or personal relationships that could have appeared to influence the work reported in this paper.

Data availability

Data will be made available on request.

Acknowledgements

This research was funded by the German Research Foundation within the priority program SPP 2364 'Autonomous Processes in Particle Technology' (Grant number: 504452366).

References

Antsaklis, P., Passino, K., Wang, S., 1991. An introduction to autonomous control systems. IEEE Control Syst. Mag. 11 (4), 5–13. https://doi.org/10.1109/37.88585. https://ieeexplore.ieee.org/abstract/document/88585.

Bi, P.-y., Li, D.-q., Dong, H.-r., 2009. A novel technique for the separation and concentration of penicillin G from fermentation broth: aqueous two-phase flotation. Sep. Purif. Technol. 69 (2), 205–209. https://doi.org/10.1016/j.seppur.2009.07.019. https://linkinghub.elsevier.com/retrieve/pii/S1383586609003116.

Bi, P.-y., Dong, H.-r., Yuan, Y.-c., 2010. Application of aqueous two-phase flotation in the separation and concentration of puerarin from Puerariae extract. Sep. Purif. Technol. 75 (3), 402–406. https://doi.org/10.1016/j.seppur.2010.09.010. https://www.sciencedirect.com/science/article/pii/S1383586610003564.

Bi, P.-Y., Chang, L., Dong, H.-R., 2011. Separation behavior of penicillin in aqueous two-phase flotation. Chin. J. Anal. Chem. 39 (3), 425–428. https://doi.org/10.1016/S1872-2040(10)60428-8. https://www.sciencedirect.com/science/article/pii/S1872204010604288.

Bi, P.-y., Chang, L., Mu, Y.-l., Liu, J.-y., Wu, Y., Geng, X., Wei, Y., 2013. Separation and concentration of baicalin from Scutellaria Baicalensis Georgi extract by aqueous two-phase flotation. Sep. Purif. Technol. 116, 454–457. https://doi.org/10.1016/j.seppur.2013.06.024. https://www.sciencedirect.com/science/article/pii/S1383586613003900.

Chang, L., Shao, Q., Xi, X., Chu, Q., Wei, Y., 2017. Separation of four flavonol glycosides from Solanum rostratum Dunal using aqueous two-phase flotation followed by preparative high-performance liquid chromatography. J. Sep. Sci. 40 (3), 804–812. https://doi.org/10.1002/jssc.201600922. eprint: https://onlinelibrary.wiley.com/doi/pdf/10.1002/jssc.201600922. https://onlinelibrary.wiley.com/doi/abs/10.1002/jssc.201600922.

Chong, K.Y., Stefanova, R., Zhang, J., Brooks, M.S.-L., 2020. Extraction of bioactive compounds from haskap leaves (Lonicera caerulea) using salt/ethanol aqueous two-phase flotation. Food Bioprocess Technol. 13 (12), 2131–2144. https://doi.org/10.1007/s11947-020-02553-3.

de Araújo Padilha, C.E., Dantas, P.V.F., Nogueira, C.d.C., de Sá Leitão, A.L., Almeida, H.N., de Santana Souza, D.F., de Oliveira, J.A., de Macedo, G.R., dos Santos, E.S., 2018. Enhancing the recovery and concentration of polyphenols from camu-camu (Myrciaria dubia H.B.K. McVaugh) by aqueous two-phase flotation and scale-up process. Sep. Sci. Technol. 53 (13), 2126–2135. https://doi.org/10.1080/01496395.2018.1442865.

Gamer, T., Hoernicke, M., Kloepper, B., Bauer, R., Isaksson, A.J., 2020. The autonomous industrial plant – future of process engineering, operations and maintenance. J. Process Control 88, 101–110. https://doi.org/10.1016/j.jprocont.2020.01.012. https://www.sciencedirect.com/science/article/pii/S0959152419305992.

Hatti-Kaul, R., 2001. Aqueous two-phase systems. Mol. Biotechnol. 19, 269–277.

Iqbal, M., Tao, Y., Xie, S., Zhu, Y., Chen, D., Wang, X., Huang, L., Peng, D., Sattar, A., Shabbir, M.A.B., Hussain, H.I., Ahmed, S., Yuan, Z., 2016. Aqueous two-phase system (ATPS): an overview and advances in its applications. Biol. Proced. Online 18 (1), 18. https://doi.org/10.1186/s12575-016-0048-8.

Jakob, L., Heinzmann, M., Nirschl, H., 2021a. Development of a continuous aqueous two-phase flotation process for the downstream processing of biotechnological products. Sep. Purif. Technol. 278, 119657. https://doi.org/10.1016/j.seppur.2021.119657. https://linkinghub.elsevier.com/retrieve/pii/S1383586621013654.

Jakob, L., Singer, J., Nirschl, H., 2021b. Importance of gas input in aqueous two-phase flotation (ATPF). Chem. Eng. Sci. 233, 116391. https://doi.org/10.1016/j.ces.2020.116391. https://linkinghub.elsevier.com/retrieve/pii/S0009250920309234.

Jakob, L., Baust, H.K., Griesinger, L., Nirschl, H., 2023. Optimized apparatus design for continuous aqueous two-phase flotation (ATPF). Separations 10 (9), 511. https://doi.org/10.3390/separations10090511. https://www.mdpi.com/2297-8739/10/9/511.

Jiang, B., Na, J., Wang, L., Li, D., Liu, C., Feng, Z., 2019a. Separation and Enrichment of Antioxidant Peptides from Whey Protein Isolate Hydrolysate by Aqueous Two-Phase Extraction and Aqueous Two-Phase Flotation. Foods 8 (1), 34. https://doi.org/10.3390/foods8010034. https://www.mdpi.com/2304-8158/8/1/34.

Jiang, B., Na, J., Wang, L., Li, D., Liu, C., Feng, Z., 2019b. Reutilization of Food Waste: One-Step Extration, Purification and Characterization of Ovalbumin from Salted Egg White by Aqueous Two-Phase Flotation. Foods 8 (8), 286. https://doi.org/10.3390/foods8080286. https://www.mdpi.com/2304-8158/8/8/286.

Jiang, B., Wang, L., Na, J., Zhang, X., Yuan, Y., Liu, C., Feng, Z., 2020. Environmentally-friendly strategy for separation of α-lactalbumin from whey by aqueous two phase flotation. Arab. J. Chem. 13 (1), 3391–3402. https://doi.org/10.1016/j.arabjc.2018.11.013. https://www.sciencedirect.com/science/article/pii/S1878535218302430.

Jiang, B., Wang, L., Wang, M., Wu, S., Wang, X., Li, D., Liu, C., Feng, Z., Chi, Y., 2021. Direct separation and purification of α-lactalbumin from cow milk whey by aqueous two-phase flotation of thermo-sensitive polymer/phosphate. J. Sci. Food Agric. 101 (10), 4173–4182. https://doi.org/10.1002/jsfa.11055. eprint: https://onlinelibrary.wiley.com/doi/pdf/10.1002/jsfa.11055. https://onlinelibrary.wiley.com/doi/abs/10.1002/jsfa.11055.

Lee, S.Y., Khoiroh, I., Ling, T.C., Show, P.L., 2016. Aqueous two-phase flotation for the recovery of biomolecules. Separation and Purification Reviews 45 (1), 81–92. https://doi.org/10.1080/15422119.2015.1007147. http://www.tandfonline.com/doi/full/10.1080/15422119.2015.1007147.

Li, M., Dong, H.-r., 2010. The investigation on the aqueous two-phase floatation of lincomycin. Sep. Purif. Technol. 73 (2), 208–212. https://doi.org/10.1016/j.seppur.2010.04.002. https://linkinghub.elsevier.com/retrieve/pii/S1383586610001395.

Lin, Y.K., Show, P.L., Yap, Y.J., Tan, C.P., Ng, E.-P., Ariff, A.B., Mohamad Annuar, M.S.B., Ling, T.C., 2015. Direct recovery of cyclodextringlycosyltransferase from Bacillus cereus using aqueous two-phase flotation. J. Biosci. Bioeng. 120 (6), 684–689. https://doi.org/10.1016/j.jbiosc.2015.04.013. https://www.sciencedirect.com/science/article/pii/S1389172315001632.

Md Sidek, N.L., Tan, J.S., Abbasiliasi, S., Wong, F.W.F., Mustafa, S., Ariff, A.B., 2016. Aqueous two-phase flotation for primary recovery of bacteriocin-like inhibitory substance (BLIS) from Pediococcus acidilactici Kp10. J. Chromatogr. B 1027, 81–87. https://doi.org/10.1016/j.jchromb.2016.05.024. https://www.sciencedirect.com/science/article/pii/S1570023216303282.

Pakhale, S.V., Vetal, M.D., Rathod, V.K., 2013. Separation of bromelain by aqueous two phase flotation. Sep. Sci. Technol. 48 (6), 984–989. https://doi.org/10.1080/01496395.2012.712596.

Ribeiro, S.C., Monteiro, G.A., Cabral, J.M.S., Prazeres, D.M.F., 2002. Isolation of plasmid DNA from cell lysates by aqueous two-phase systems. Biotechnol. Bioeng. 78 (4), 376–384. https://doi.org/10.1002/bit.10227. eprint: https://onlinelibrary.wiley.com/doi/pdf/10.1002/bit.10227. https://onlinelibrary.wiley.com/doi/abs/10.1002/bit.10227.

Rito-Palomares, M., Benavides, J. (Eds.), 2017. Aqueous Two-Phase Systems for Bioprocess Development for the Recovery of Biological Products. Food Engineering Series. Springer International Publishing, Cham. http://link.springer.com/10.1007/978-3-319-59309-8.

Sankaran, R., Show, P.L., Yap, Y.J., Lam, H.L., Ling, T.C., Pan, G.-T., Yang, T.C.-K., 2018. Sustainable approach in recycling of phase components of large scale aqueous two-phase flotation for lipase recovery. J. Clean. Prod. 184, 938–948. https://doi.org/10.1016/j.jclepro.2018.02.301. https://linkinghub.elsevier.com/retrieve/pii/S0959652618306395.

Sankaran, R., Parra Cruz, R.A., Show, P.L., Haw, C.Y., Lai, S.H., Ng, E.-P., Ling, T.C., 2019. Recent advances of aqueous two-phase flotation system for the recovery of biomolecules. Fluid Phase Equilib. 501, 112271. https://doi.org/10.1016/j.fluid.2019.112271. https://linkinghub.elsevier.com/retrieve/pii/S0378381219303322.

Show, P.L., Tan, C.P., Anuar, M.S., Ariff, A., Yusof, Y.A., Chen, S.K., Ling, T.C., 2011. Direct recovery of lipase derived from Burkholderia cepacia in recycling aqueous two-phase flotation. Sep. Purif. Technol. 80 (3), 577–584. https://doi.org/10.1016/j.seppur.2011.06.013. https://linkinghub.elsevier.com/retrieve/pii/S1383586611003510.

Show, P.L., Ooi, C.W., Anuar, M.S., Ariff, A., Yusof, Y.A., Chen, S.K., Annuar, M.S.M., Ling, T.C., 2013. Recovery of lipase derived from Burkholderia cenocepacia ST8 using sustainable aqueous two-phase flotation composed of recycling hydrophilic organic solvent and inorganic salt. Sep. Purif. Technol. 110, 112–118. https://doi.org/10.1016/j.seppur.2013.03.018. https://linkinghub.elsevier.com/retrieve/pii/S1383586613001561.

Torres-Acosta, M.A., Mayolo-Deloisa, K., González-Valdez, J., Rito-Palomares, M., 2019. Aqueous two-phase systems at large scale: challenges and opportunities. Biotechnol. J. 14 (1), 1800117. https://doi.org/10.1002/biot.201800117.

eprint: https://onlinelibrary.wiley.com/doi/pdf/10.1002/biot.201800117. https://onlinelibrary.wiley.com/doi/abs/10.1002/biot.201800117.

Wallén, A., 2000. Tools for Autonomous Process Control. Doctoral Thesis (monograph). Department of Automatic Control, Lund Institute of Technology (LTH).

Xu, M., Finch, J.A., Uribe-Salas, A., 1991. Maximum gas and bubble surface rates in flotation columns. Int. J. Miner. Process. 32 (3), 233–250. https://doi.org/10.1016/0301-7516(91)90070-Y. https://www.sciencedirect.com/science/article/pii/030175169190070Y.